Microscopy using non uniform polarization

Author: Marcos Pérez Aviñoa
*Facultat de Física, Universitat de Barcelona, Diagonal 645, 08028 Barcelona, Spain.**

Advisor: Artur Carnicer
(Dated: Compiled January 15, 2018)

In this work we study the effects of non uniform polarization in microscopy. Based on electromagnetic diffraction, we develop an imaging theory for high numerical aperture systems. A vortex filter is placed in the back focal plane of the objective. Assuming linear input polarization, we characterise the transfer functions and point spread functions of the system with and without the filter. A study of totally incoherent light is also made. Finally, experimental results are shown for each polarization and coherency case.

I. INTRODUCTION

In searching for higher resolution images through a microscope a dramatic increase in their numerical aperture (NA) was unavoidable. The assumptions of the scalar diffraction theory broke down as the incoming rays neared the 90 degree mark. Richards and Wolf laid the basis of electromagnetic diffraction in an optical system in [1]. This theory initially succeeded in the determination of the electric field in the focal region of a lens, where the polarization plays a central role, as each component of the electromagnetic field interferes with each other.

As the discrepancies arose, the interest in image formation under a microscope increased. Sheppard and Wilson [2] determined the image of an object illuminated by a plane wave, assuming it radiates as a dipole. This approach effectively determines the point spread function of the system (PSF). The light distribution in the image plane depends on both the pattern of the illuminating aperture and the NA of the objective. Under circular apertures, the effect of the high NA is to decrease the contrast between minima and maxima of the PSF. Such an approach is treated in modern terms in [3].

A more rigorous approach to the image formation in a microscope can be found in [4]. Although more precise, the difference in the approach is in the interaction of light with the object. No assumptions are made and an FDTD method is used to account for light scattering.

Sheppard has also studied the effects of the NA on the transfer functions of a lens, both in the scalar [5] and vectorial case [6]. Their studies are quite general, taking into account narrowband light. Both studies state the clear differences between paraxial and non paraxial theory, starting by the need of a three dimensional transfer function for the complete determination of the lens.

With the advent of higher resolution spatial light modulators, interesting techniques have been suggested for optical microscopy. In particular, the use of a vortex phase filter can enhance the edges of the input image [7–9]. Recently, edge detection has been improved with the aid of polarized beams [10–12]. A vortex filter acts in a similar way as the phase one, but weighs its effects between polarization components. This produces edges that are polarized depending on the optical vortex produced by the filter. Provided the incident polarization onto said filter, the directions of the edges can be retrieved by a simple use of a linear polarizer.

This work focuses on the image formation through a high NA system, both in the coherent and incoherent cases. A general theory is derived on the basis of electromagnetic diffraction but without dwelling into the exact mode of radiation of the illuminated sample. The radiated field is proportional to the shape of the sample, an approach that corresponds to the First Born approximation. In the Fourier plane of the objective a vortex filter is placed to generate polarized beams.

The structure of this work is as follows: the first section lays out the electromagnetic diffraction theory and the characteristics of the filter. Then, we study the coherent and incoherent transfer functions. After that, the experimental set-up and results are discussed. We finish with some concluding remarks.

II. THEORETICAL BASIS

We are set to model the light propagation through a high NA microscope. A schematic view of such system is presented in FIG. 1. The fields $\mathbf{E}_1$ and $\mathbf{E}_2$ correspond to

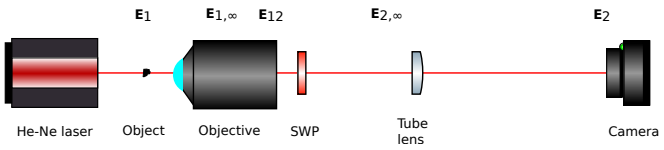

FIG. 1: Diagram of the electric fields in the microscope. $\mathbf{E}_{12}$ represents the field after the objective.

the object plane and image plane respectively, with $\mathbf{E}_{\infty,1}$ and $\mathbf{E}_{\infty,2}$ being their fields at infinity, in the Gaussian reference sphere. $\mathbf{E}_{12}$ is the intermediate field at the tube of the microscope. The azimuthal unit vector is

*Electronic address: mperezav7@alumnes.ub.edu

common along the system, while the two lenses have a different maximum aperture angle θ. The unit vectors are, expressed in Cartesian coordinates:

$$\begin{aligned}\mathbf{e}_\rho &= (\cos\varphi, \sin\varphi, 0)\\ \mathbf{e}_\varphi &= (-\sin\varphi, \cos\varphi, 0)\\ \mathbf{e}_{\theta_i} &= (\cos\theta_i\cos\varphi, \cos\theta_i\sin\varphi, \sin\theta_i)\end{aligned} \tag{1}$$

where $i = 1, 2$.

The electromagnetic diffraction theory developed by Richards and Wolf [1] relates the intermediate field $\mathbf{E}_{12}$ with the one at the focal region of the objective by means of the integral:

$$\mathbf{E}_1 = C\iint_\Sigma \mathbf{E}_{\infty,1} \mathrm{e}^{ik(r\sin\theta_1\cos(\phi-\varphi)+z\cos\theta_1)}\sin\theta_1 d\theta_1 d\varphi \tag{2}$$

where Σ is the lens extent, z the distance from the focal plane, θ_1 and ϕ are the coordinates at the focal plane, r and φ, the coordinates at the Gaussian reference sphere and C is a constant. This integral can be written as a Fourier transform relation [13]:

$$\mathbf{E}_1 = \mathrm{FT}^{-1}_{\lambda f}\left[\frac{\mathbf{E}_{\infty,1}}{\cos\theta_1}\exp(-ikz\cos\theta_1)\right] \tag{3}$$

where the finite extent of the lens has been included in the definition of $\mathbf{E}_1$ Given the conservation of energy through the lens and the refraction of the rays at its surface, the field at the Gaussian reference sphere can be related to the one in the tube:

$$\mathbf{E}_{\infty,1} = \sqrt{\cos\theta_1}[(\mathbf{E}_{12}\cdot\mathbf{e}_\varphi)\mathbf{e}_\varphi + (\mathbf{E}_{12}\cdot\mathbf{e}_\rho)\mathbf{e}_{\theta_1}] \tag{4}$$

In image formation we are interested in the field $\mathbf{E}_2$ in the image plane produced by $\mathbf{E}_1$, the field of the object. Using 3 we invert the relationship between the two:

$$\mathbf{E}_{\infty,1} = \cos\theta_1\exp(ikz\cos\theta_1)\mathrm{FT}_{\lambda f}[\mathbf{E}_1] \tag{5}$$

Following a reasoning similar to Sheppard [2], the inversion of the refraction at the Gaussian reference sphere is given by:

$$\mathbf{E}_{12} = (\cos\theta_1)^{-1/2}[(\mathbf{E}_{\infty,1}\cdot\mathbf{e}_\varphi)\mathbf{e}_\varphi + (\mathbf{E}_{\infty,1}\cdot\mathbf{e}_{\theta_1})\mathbf{e}_\rho] \tag{6}$$

Propagation to the image plane can be done by direct use of 3, substituting $\mathbf{E}_1$ by $\mathbf{E}_2$ and $\mathbf{E}_{\infty,1}$ by $\mathbf{E}_{\infty,2}$, which is given by the relation 4 changing 1 by 2 in the expression.

Since the region of the tube is paraxial, the field $\mathbf{E}_{12}$ is described just by the two transversal components of propagation, $\mathbf{E}_{12} = (E_x, E_y)$. As this analysis assumes coherent fields, propagation in this region can be taken into account using the Jones formulation. In particular, this allows us to describe the effects of an spiral wave plate in this region using the matrix:

$$\mathbf{M}_{swp} = \begin{pmatrix}\cos\varphi & \sin\varphi\\ -\sin\varphi & \cos\varphi\end{pmatrix} \tag{7}$$

Since now the field propagates as a whole, the effect of the system onto each component may be different. Going back to the theory of linear systems, we study the effect of the system onto the vectorial light distribution in the object by its PSF. We define it as the response of our system to a point source. For simplicity, we assume a mathematical point of the form $\mathbf{E}_{point}(x, y, z = 0) = \mathbf{A}\delta(x, y)$ where $\mathbf{A}$ is a constant polarization vector and $\delta(x, y)$ is the Dirac delta function, avoiding the physical description of a point light source.

With coherent illumination, every surface and speck of dust acts as an interference or diffraction source which add to the ideal image of the object. Spatially incoherent light averages out this effects and potentially offers a better image quality. For this reason, we also study its effects onto the image formation under high NA.

A comprehensive study would analyse the image field with varying complex degree of cohrence of the light incident on the object. Such an approach is out of the scope of this work and we refer to the results derived in [14] for totally incoherent light. Under this condition, we can relate the image and object intensities, I_i and I_o respectively, by a convolution by the modulus squared of the PSF. Using the convolution theorem:

$$\begin{aligned}I_i &= FT^{-1}[\mathcal{H}FT[I_o]]\\ \mathcal{H} &\equiv \frac{\iint_{-\infty}^{\infty}|\mathbf{h}|^2\mathrm{e}^{-2\pi i(ux+vy)}dxdy}{\iint_{-\infty}^{\infty}|\mathbf{h}|^2dxdy}\end{aligned} \tag{8}$$

where $\mathcal{H}$ is the normalized optical transfer function (OTF). Its modulus is called modulus transfer function (MTF). Now, each component of the transfer function adds linearly to the total, as opposed to the coherent case. The resulting intensity can be determined just by a scalar function alone, although at a loss of information about polarization.

III. NUMERICAL CALCULATIONS

We analyse the numerical results of the theory laid in the section II. First we mention the coherent properties of the PSF, the incoherent OTF and then we highlight the most interesting result. In TABLE I we have all the data used to calculate the PSF of the system. The two different L used for the object region are used to get a better resolution of the PSF or the amplitude transfer function, respectively.

N	L	f_1	f_2	NA
2048	8-200λ	5mm	200 mm	0.75

TABLE I: **Data used in the calculation of the PSF. N is the number of pixels, L is the half width of the sampling region in the object plane, f_1 and f_2 are the objective and tube lens focal lengths and NA is the numerical aperture.**

A. Coherent properties

We consider a delta point source of light, as stated in section II, and linear polarization, $\mathbf{A} = (1, 0, 0)$. When macroscopic results are presented, the dimensions will be displayed in millimetres, assuming in all cases $\lambda = 500$nm. To generate radial polarization, we will assume that the light remains linearly polarized after passing through the objective.

The intensity for each component and the total is shown at FIG. 2. (a) and (b) are the x and y components of the radially polarized light and (c) their modulus squared sum. The PSF presents a zero value of intensity at its center, much unlike the case of linear polarized light, present in (f). Even for this case, clear discrepancies can be seen in (d) and (e): the x component is elongated in the direction perpendicular to the polarizarion and there exists a non zero y component, although it only accounts to a 3% of the energy.

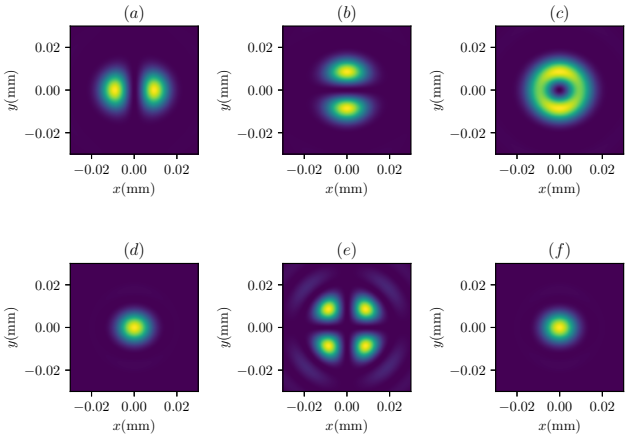

FIG. 2: Modulus squared of the PSF. Upper row and lower row correspond to radial and linear polarizations respectively. (a) and (d) are the x-components and (b) and (e), the y-components. (c) and (f) are the total intensities of the PSF for each polarization.

More interesting results appear upon examination of the amplitude transfer function. Only the x components will be shown, as the other one is negligible in linear polarization and, in the case of radial polarization, it is the same but rotated 90 degrees. In (d) from FIG. 3 we see that the classical predictions do not hold: the function is not constant over the aperture of the system and, like the PSF, is elongated perpendicular to the direction of polarization. In (c) it can bee seen that, for low frequencies, the function can be considered almost constant, coinciding with the predictions of the paraxial theory. The results of radial polarization need careful examination. The transfer function is of the form $\mathbf{H} \propto (\cos\varphi, \sin\varphi)$ and each component varies on the circle as can be seen on (b). (c) shows a dip at its centre produced by the discontinuity of the azimuthal angle near the origin. We can see this by writing the cosine function as $\cos\varphi = \frac{\mathrm{sgn}(x)}{\sqrt{1+y^2/x^2}}$ This behaviour makes the transfer function of the radial polarization an extremely narrow high pass function near the origin. Light passing through such a filter will see only its lowest frequency components removed upon propagation. This means that the background light and constant large contrast regions will be removed in the image plane.

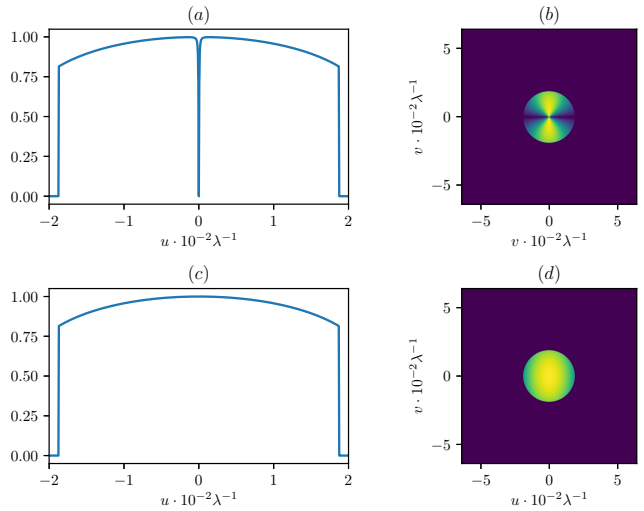

FIG. 3: Modulus of the amplitude transfer function. Upper row corresponds to radial polarization and lower, to linear polarization.(a) and (c) show a profile of the modulus and (b) and (d), a map of their values.

B. Incoherent properties

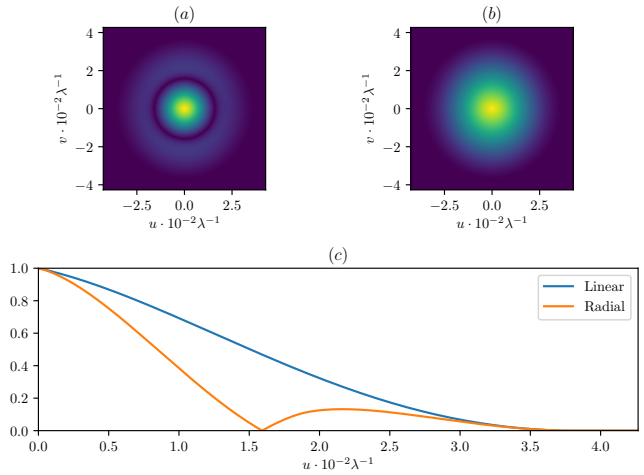

FIG. 4: MTFs of both radial polarization (a), linear polarization (b), and their profile comparison (c).

As stated above, once determined the PSF of the system we can readily generate its OTF. In FIG. 4 we can see that the MTFs of linear and radial polarization show some clear differences with respect to their amplitude transfer function counterparts. Firstly, (a) and (b) show that the functions are no longer almost constant through the allowed frequency range. Secondly, their domain has doubled, allowing for more frequencies to pass, although with decreasing intensity, as seen in (c). This increase of resolution only applies to pure or nearly pure amplitude objects, since the phase information cannot be transmitted as the illumination makes the system linear in intensity.

Between the linear and radial polarized cases there is a clear difference: the latter presents a point where its MTF is null. This point is the radius of the cutoff frequency of the amplitude transfer function. The frequencies near this point will not be transmitted through the system. Moreover, this point marks a sign change in the OTF, meaning that an inversion contrast will be seen for the higher frequencies. For this to happen, we see that the radial MTF falls off rapidly than the linear for the lower frequencies. All in all, we can expect that with incoherent radially polarized light a worse image than with linear case.

C. Discussion

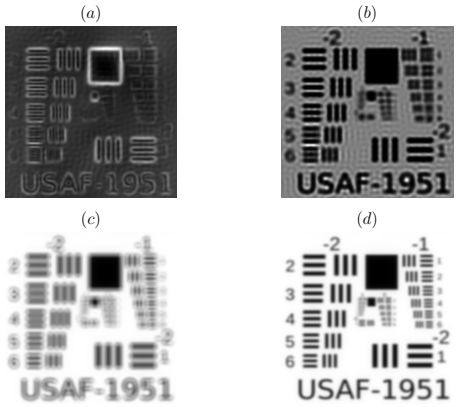

FIG. 5: USAF test imaging using different polarizations and coherency states. The upper row is coherent illumination and the lower incoherent. (a) and (c) correspond to radial polarization and (b) and (d) to linear.

The transfer function for radial polarization shows a very interesting result: the value at its centre is zero. This, in turn, creates an extremely narrow high pass filter that removes the energy of the image and only the edges remain. This can be seen in FIG. 4 (a). Unfortunately, this feature is not present in incoherent illumination since the OTF for radial polarization does not go to zero at the origin and a contrast inversion occurs, lowering the overall image quality.

In FIG. 5 the results of a simulation under the conditions discussed is shown. The edge detection can be seen comparing (a) with (b). Although (c) is radially polarized, the incoherent light does not allow the edge detection and, upon comparing with (d), a clear reduction of the quality of the image is seen. The practical interest of radial polarization lays entirely on its coherent properties.

IV. EXPERIMENTAL SET-UP AND RESULTS

Ideally, we would test the numerical results constructing a system as described in Section II, but the back focal plane of the high NA microscope we disposed could not be accessed. In Tabale II we present the specifications of our experimental system. The main difference is that the transfer functions are more paraxial and, therefore, more symmetric with respect to the central axis. Also, due to technical limitations, we can only test coherent and incoherent cases in radial polarization.

The sample is illuminated by a He-Ne laser passing through a collimation system. In the collimated zone, we place a diffuser to switch between coherent and incoherent illumination.

f_1	NA	f_2	n_x	n_y	Bit depth
5 mm	0.45	200 mm	1292	964	14 bit

TABLE II: **Experimental data of the system. f_i are the focal lengths of the objective and the tube lens, NA is the numerical aperture of the objective and n_i are the number of pixels of the camera, with its bit depth.**

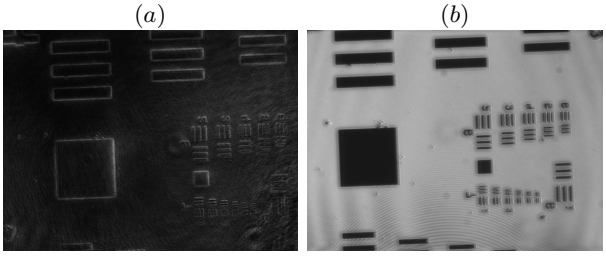

FIG. 6: Experimental images of a USAF resolution chart with both coherent (a) and incoherent (b) light under the effects of a radial polarizer.

The object used is an USAF resolution chart, placed in the front focal plane of the ojective. Both coherent and incoherent illumination are used. The SWP is placed in the back focal plane of the objective. In FIG. 6 we show the images recorded. Even though the frequencies are too low to see the low pass filtering of the pupil of the

system and despite the high coherent noise, the theory here exposed holds. The image in (a) has an appreciable intensity only where the edges of the bars are and in contrast with (b), where the zero order of light is present.

V. CONCLUSIONS

Using the electromagnetic diffraction theory, we have derived a systematic approach to image formation under high NA systems, similar to the classical linear system approach. The object is illuminated by a He-Ne laser linearly polarized. A SWP is put at the back focal plane of the objective to produce radially polarized light. For both coherent and incoherent cases, the effect of the high NA is to elongate the transfer functions and OTFs in the direction perpendicular to the input polarization and to create a transverse and longitudinal components, decreasingly in importance. The main direction of polarization still accounts for over 97% of the energy.

In the coherent case, each component of the PSFs is also elongated. The SWP acts as an extemely narrow high pass filter, which in turn produces a doughnut shaped PSF. The transfer functions are non constant and decrease with increasing spatial frequency.

In the incoherent case, the main difference with the classical theory appears with the radial polarization. The OTF presents a contrast inversion, which in turn forces it to decrease more rapidly in the lower frequencies. Its overall effect is to lower image quality.

Acknowledgments

I would like to thank Artur Carnicer and Ignasi Juvells for offering me this opportunity, Santiago Vallmitjana for all his tips and help in the laboratory, my family and friends for all their support and especially Victòria, for always being there when I need it.

[1] B. Richards and E. Wolf, "Electromagnetic diffraction in optical systems II. structure of the image field in an aplanatic system," *Proceedings of the Royal Society A*, vol. 253, pp. 359–379, December 1981.

[2] C. Sheppard and T. Wilson, "The image of a single point in microscopes of large numerical aperture," *Proceedings of the Royal Society A*, vol. 379, pp. 145–158, January 1981.

[3] L. Novotny and B. Hecht, *Principles of Nano-Optics*. Cambridge University Press, 2nd ed., 2012.

[4] P. Török, P. Munro, and E. Kriezis, "High numerical aperture vectorial imaging in coherent optical microscopes," *Optics Express*, vol. 16, no. 2, 2008.

[5] C. Sheppard, M. Gu, Y. Kawata, and S. Kawata, "Three-dimensional transfer functions for high-aperture systems," *Journal of the Optical Society of America A*, vol. 11, no. 2, pp. 593–598, 1994.

[6] C. Sheppard and K. Larking, "Vectorial pupil functions and vectorial transfer functions," *Optik*, vol. 107, no. 2, pp. 79–87, 1997.

[7] S. Fürhapter, A. Jesacher, S. Bernet, and M. Ritsch-Marte, "Spiral phase contrast imaging in microscopy," *Optics Express*, vol. 13, February 2005.

[8] S. Bernet, A. Jesacher, S. Fürhapter, C. Maurer, and M. Ritsch-Marte, "Quantitative imaging of complex samples by spiral phase contrast microscopy," *Optics Express*, vol. 14, no. 9, 2006.

[9] C. Guo, Y. Han, and J. Xu, "Radial Hilbert transform with Laguerre-Gaussian spatial filters," *Optics Letters*, vol. 31, May 2006.

[10] Y. Han, C. Guo, Z. Rong, and L. Chen, "Radial Hilbert transform with the spatially variable half-wave plate," *Optics Letters*, vol. 38, no. 23, pp. 5169–5171, 2013.

[11] B. Zhang, Z. Chen, H. Sun, J. Xia, and J. Ding, "Vectorial optical vortex filtering for edge enhancement," *Journal of Optics*, vol. 18, no. 3, p. 035703, 2016.

[12] B. Bhargava Ram, P. Senthilkumaran, and A. Sharma, "Polarization-based spatial filtering for directional and nondirectional edge enhancement using an s-waveplate," *Applied optics*, vol. 56, April 2017.

[13] A. Carnicer, I. Juvells, B. Javidi, and R. Martínez-Herrero, "Optical encryption in the longitudinal domain of focused fields," *Optics Express*, vol. 24, no. 7, pp. 6793–6801, 2016.

[14] J. W. Goodman, *Introduction to Fourer Optics*. McGraw-Hill, 3rd ed., 2005.